

Parameterisation of Radiation Forces for a Multiple Degree-of-Freedom Wave Energy Converter Using Moment-Matching

Nicolás Faedo, Yerai Peña-Sanchez and John V. Ringwood
Centre for Ocean Energy Research, Maynooth University, Maynooth, Ireland

ABSTRACT

The motion of a Wave Energy Converter (WEC) can be described in terms of an integro-differential equation, which involves a convolution operator. This convolution term accounts for the effect of radiation forces acting on the device, and represents a computational and representational drawback both for simulation, and analysis/design of control/estimation strategies. We present herein a moment-based strategy to compute a parametric form of the radiation force subsystem for multiple degree of freedom WECs. The strategy allows for the computation of a model that *exactly* matches the steady-state behaviour of the target system at a set of user-defined frequencies, while retaining the underlying physical properties of radiation forces. The potential and capabilities of the presented method are illustrated considering a CorPower-like device (heaving point absorber) as an application case.

KEY WORDS: Radiation forces; Parametric form; Model order reduction; Frequency-domain identification; Moment-matching

INTRODUCTION

While limited by the linear nature of potential flow theory, the speed with which numerical simulation may be performed makes the widely-known Boundary Element Method (BEM) a common choice to compute hydrodynamic parameters for a given Wave Energy Converter (WEC) (Penalba et al., 2017). However, one of the major drawbacks of BEMs is that the results are computed in the frequency domain and, hence, can only characterise the steady-state motion of the WEC under analysis. Seeking for a more comprehensive approach, and following the well-known theory developed in (Cummins, 1962), the motion of a WEC can be expressed, in the time domain, using a particular well-known integro-differential equation of the convolution class. The presence of these convolution terms account for the effect of radiation forces acting on each of the different degrees of freedom (DoF) of the device, constituting a (hydrodynamic) coupling between these modes of motion.

The existence of these convolution terms represents a significant drawback both for motion simulation, and for modern analysis/design of control/estimation strategies. From a motion simulation point of view, it is well-known that the explicit computation of the convolution operator is computationally inefficient, often worsened by the necessity of a small (time) discretisation step to obtain accurate numerical integration. From a control/estimation theory point of view, the presence of these convolution mappings complicates the application of well-established results in the field, since modern control/estimation techniques are based on the availability of a state-space representation (at least in local coordinates) of the system under analysis (Faedo et al., 2017). Motivated by these drawbacks, researchers often seek for a parametric approximation of this radiation force subsystem in terms of a linear time-invariant dynamical representation, making explicit use of the corresponding hydrodynamic characteristics of the device obtained from BEM solvers. By way of example, in the case of control applications, studies that consider this approximation modality can be found in (Hals et al., 2011, Li and Belmont, 2014) while, for the estimation case, (Peña-Sanchez et al., 2018) implements this same strategy.

To be precise, the prevailing approach is to approximate each convolution term independently (see, for example, (Giorgi and Ringwood, 2019, Li and Belmont, 2014)), as a single-input single-output (SISO) dynamical system, even though the problem is inherently multiple-input multiple-output (MIMO), as a consequence of the multi-DoF characteristic of the WEC. One main disadvantage of this “multi-SISO” approach is that treating each convolution term independently often leads to an unnecessary high-order dimensional parameterisation of the radiation force subsystem, potentially rendering any control/estimation strategy challenging for real-time applications (Faedo et al., 2017).

We have recently presented a moment-matching-based MIMO identification method for wave energy applications in (Peña-Sanchez et al., 2019), particularly to approximate the response of an array of WECs, i.e. a “farm” of multiple 1-DoF devices. This strategy is based on the underlying theoretical concepts developed in (Faedo et al., 2018b), and allows for the computation of a model that *exactly* matches the frequency response of the target

MIMO system at a set of user-selected frequencies \mathcal{F} , providing an efficient and accurate method to compute a state-space representation for the WEC dynamics. Additionally, and as discussed in (Faedo et al., 2018b), a wise selection of the set \mathcal{F} within this moment-based approach, helps to enforce the underlying (physical) properties of the WEC under analysis.

Motivated by these results, in this paper, we present an adaptation of the MIMO identification framework developed in (Peña-Sanchez et al., 2019) to compute a parametric approximation of the radiation force subsystem of a multi-DoF device. We demonstrate that treating the approximation of radiation forces with our MIMO moment-based strategy (instead of the usual “multi-SISO” approach) provides a highly accurate low dimensional system, hence offering a reliable parametric model, while also reducing the computational effort required for time-domain simulations and control/estimation calculations. Moreover, we show that we can guarantee essential physical properties of radiation forces in the approximating model, such as bounded-input, bounded-output (BIBO) stability.

The remainder of this paper is organised as follows. Section 2 recalls the theory behind moment-matching for MIMO systems. Section 3 briefly discusses modelling of multi-DoF WECs in both the time and frequency domains. Section 4 presents a moment-domain analysis of radiation forces, while Section 5 discusses a moment-based algorithm to compute a parametric approximation for the radiation force subsystem of a multi-DoF WEC. Section 6 discusses an application case, where a CorPower-like device (heaving point absorber) is considered. Finally, Section 7 encompasses the main conclusions of this study.

Notation and Preliminaries

Standard notation is considered through this study, with any exceptions detailed in this section. \mathbb{R}^+ (\mathbb{R}^-) denotes the set of non-negative (non-positive) real numbers. \mathbb{C}^0 denotes the set of pure-imaginary complex numbers and $\mathbb{C}_{<0}$ denotes the set of complex numbers with a negative real part. The symbol 0 stands for any zero element, dimensioned according to the context. The symbol \mathbb{I}_n denotes an order n identity matrix. The spectrum of a matrix $A \in \mathbb{R}^{n \times n}$, i.e. the set of its eigenvalues, is denoted as $\lambda(A)$. The notation W^\dagger , with $W \in \mathbb{R}^{n \times m}$, denotes the *Moore-Penrose* inverse of W . The symbol \bigoplus denotes the direct sum of n matrices, i.e. $\bigoplus_{i=1}^n A_i = \text{diag}(A_1, A_2, \dots, A_n)$. The expression $\|X\|_F$ denotes the *Frobenius* norm of the matrix X . The *Kronecker product* between two matrices $M_1 \in \mathbb{R}^{n \times m}$ and $M_2 \in \mathbb{R}^{p \times q}$ is denoted as $M_1 \otimes M_2 \in \mathbb{R}^{np \times mq}$. The convolution between two functions $f(t)$ and $g(t)$ over a finite range $[0, t]$, i.e. $\int_0^t f(\tau)g(t - \tau)d\tau$ is denoted as $f(t) * g(t)$. The Fourier transform of a function $f(t) \in L^2(\mathbb{R})$ is denoted by $\mathcal{F}\{f(t)\} = \hat{f}(j\omega)$, while its Laplace transform is denoted as $\mathcal{L}\{f(t)\} = F(s)$, where $L^2(\mathbb{R}) = \left\{f : \mathbb{R} \rightarrow \mathbb{C} \mid \int_{-\infty}^{\infty} |f(t)|^2 dt < +\infty\right\}$. The symbol $e_{ij}^q \in \mathbb{R}^{q \times q}$ denotes a matrix with 1 in the ij -component and 0 elsewhere. Finally, the symbol $\varepsilon_n \in \mathbb{R}^{n \times 1}$ denotes a vector with odd components equal to 1 and even components equal to 0.

MOMENTS FOR MIMO SYSTEMS

We note that the theory recalled herein is originated within the field of *model order reduction* in (Astolfi, 2010), being adapted for the WEC identification problem in (Faedo et al., 2018b, 2019,

Peña-Sanchez et al., 2019). The interested reader is referred to (Scarciotti and Astolfi, 2017, Chapter 1) for a thorough discussion on different model order reduction techniques and, particularly, on moment-based methods.

Consider a finite-dimensional, MIMO, continuous-time system Σ described, for $t \geq 0$, by the state-space model

$$\Sigma : \begin{cases} \dot{x}(t) = Ax(t) + Bu(t), & y(t) = Cx(t), \end{cases} \quad (1)$$

with $x(t) \in \mathbb{R}^n$, $u(t) \in \mathbb{R}^q$, $y(t) \in \mathbb{R}^q$, $A \in \mathbb{R}^{n \times n}$, $B \in \mathbb{R}^{n \times q}$ and $C \in \mathbb{R}^{q \times n}$. Consider the transfer function $W : \mathbb{C} \rightarrow \mathbb{C}^{q \times q}$, computed in terms of the associated impulse response matrix $w(t) = Ce^{At}B$ with $w_{ij}(t) \in L^2(\mathbb{R})$, where $w_{ij}(t)$ denotes the ij -element of $w(t)$, as

$$\mathcal{L}\{w(t)\} \mapsto W(s) = C(s\mathbb{I}_n - A)^{-1}B, \quad (2)$$

and assume that (1) is minimal, i.e. controllable and observable¹.

Definition 1. (Antoulas, 2005) The 0-moment of system (1) at $s_i \in \mathbb{C} \setminus \lambda(A)$ is the complex matrix $\eta_0(s_i) = C(s_i\mathbb{I}_n - A)^{-1}B$. The k -moment of system (1) at $s_i \in \mathbb{C}$ is the complex matrix

$$\eta_k(s_i) = \frac{(-1)^k}{k!} \left[\frac{d^k}{ds^k} W(s) \right]_{s=s_i}, \quad (3)$$

with $k \geq 1$ integer.

Remark 1. Note that moments, as in Definition 1, are the coefficients of the Laurent expansion of the transfer function $W(s)$ around the complex point s_i .

Remark 2. The idea of the moment-based model order reduction technique is based on interpolating the transfer function of the original system (and the derivatives of this) and the transfer function of the reduced order model (and the derivatives of this) at these interpolation points s_i .

The pioneering study (Astolfi, 2010) shows that the moments of a SISO linear system are in a one-to-one relation with the steady-state response (provided it exists) of the output of the interconnection between a signal generator and the system Σ itself. This concept is formally extended to MIMO systems in (Faedo et al., 2019, Peña-Sanchez et al., 2019), and briefly recalled in the following theorem.

Theorem 1. (Faedo et al., 2019, Peña-Sanchez et al., 2019) Consider system (1) and the autonomous multiple-output signal generator

$$\mathcal{G} : \begin{cases} \dot{\Xi}(t) = (\mathbb{I}_q \otimes S)\Xi(t), & u(t) = L\Xi(t), \end{cases} \quad (4)$$

with $\Xi(t) \in \mathbb{R}^{q\nu}$, $S \in \mathbb{R}^{\nu \times \nu}$, $L \in \mathbb{R}^{q \times q\nu}$, $\Xi(0) \in \mathbb{R}^{q\nu}$, $\lambda(A) \subset \mathbb{C}_{<0}$, $\lambda(S) \subset \mathbb{C}^0$ and the eigenvalues of S are simple. Suppose the triple of matrices $(L, \mathbb{I}_q \otimes S, \Xi(0))$ is minimal. Let $\Pi \in \mathbb{R}^{n \times q\nu}$ be the (unique) solution of the Sylvester equation

$$A\Pi + BL = \Pi(\mathbb{I}_q \otimes S). \quad (5)$$

Then, there exists a one-to-one relation between the moments $\eta_0(s_1), \eta_0(s_2), \dots, \eta_0(s_\nu)$, with $s_i \in \lambda(S)$ for all $i \in \mathbb{N}_\nu$, and the steady-state response $C\Pi\Xi$ of the output y of the interconnection of system (1) with the signal generator (4).

Remark 3. The minimality of the triple $(L, \mathbb{I}_q \otimes S, \Xi(0))$ implies the observability of the pair $(L, \mathbb{I}_q \otimes S)$ and the *excitability*² of the pair $(\mathbb{I}_q \otimes S, \Xi(0))$.

¹The reader is referred to (Khalil, 1996) for further detail on the concept of controllability and observability of a dynamical system.

²We refer the reader to (Padoan et al., 2017) for the definition of excitability.

Remark 4. From now on, we refer to the matrix $C\Pi \equiv \underline{\mathcal{Y}}$, with Π the solution of (5), as the *moment-domain equivalent* of $y(t)$.

Following this steady-state interpretation of moments, we now recall from (Astolfi, 2010) the formal definition of a reduced order model achieving moment-matching for system (1).

Definition 2. (Astolfi, 2010) Consider system (1) and the signal generator (4). The system described by the equations

$$\Sigma_{\mathcal{G}} : \{\dot{\Theta}(t) = F\Theta(t) + Gu(t), \quad \theta(t) = Q\Theta(t), \quad (6)$$

with $\Theta \in \mathbb{R}^{q\nu}$, $\theta(t) \in \mathbb{R}^q$, $F \in \mathbb{R}^{q\nu \times q\nu}$, $G \in \mathbb{R}^{q\nu \times q}$ and $Q \in \mathbb{R}^{q \times q\nu}$ is a model of system (1) at S if system (6) has the same moments at S as system (1).

Lemma 1. (Astolfi, 2010) Consider system (1) and the signal generator (4). Then, the system defined in (6) is a model of system (1) at S if $\lambda(F) \cap \lambda(S) = \emptyset$ and

$$\underline{\mathcal{Y}} = QP, \quad (7)$$

where $\underline{\mathcal{Y}} = C\Pi$ is the moment-domain equivalent of the output of system (1) computed from (5), and P is the unique solution of the Sylvester equation

$$FP + GL = P(\mathbb{I}_q \otimes S). \quad (8)$$

Remark 5. The transfer function of system $\Sigma_{\mathcal{G}}$ interpolates the transfer function of system Σ at the eigenvalues of the matrix S . Equivalently, the steady-state output of the reduced order model (6) exactly matches the steady-state output of the system resulting from the interconnection of systems (1) and (4).

Given the characteristics of $\lambda(S)$ in Theorem 1, we set a standing assumption on the matrix S and we recall a useful lemma from (Faedo et al., 2019), which provides an alternative path for the computation of the matrix $\underline{\mathcal{Y}} = C\Pi$, in terms of the impulse response matrix of system Σ .

Assumption 1. Consider the finite set $\mathcal{F} = 0 \cup \{\omega_p\}_{p=1}^f \subset \mathbb{R}^+$. The matrix S in (4) is written in block-diagonal form as

$$S = 0 \oplus \left(\bigoplus_{p=1}^f \begin{bmatrix} 0 & \omega_p \\ -\omega_p & 0 \end{bmatrix} \right), \quad (9)$$

where $\nu = 2f + 1$, $f \geq 0$ integer.

Lemma 2. (Faedo et al., 2019, Peña-Sanchez et al., 2019) Consider the interconnection between system (1) and the signal generator (4), and suppose Assumption 1 holds. Without losing generality, assume that $\Xi(0) = [1 \ e_{\nu-1}^T]^T$ so that the minimality of the triple $(L, \mathbb{I}_q \otimes S, \Xi(0))$ holds as long as the pair $(L, \mathbb{I}_q \otimes S)$ is observable. Then, the moment-domain equivalent $\underline{\mathcal{Y}}$ can be computed from the impulse response of system (1) as

$$\underline{\mathcal{Y}} = \sum_{i=1}^q \sum_{j=1}^q e_{ij}^q L (\mathbb{I}_q \otimes \mathcal{R}_{ij}^w), \quad (10)$$

where each $\mathcal{R}_{ij}^w \in \mathbb{R}^{\nu \times \nu}$ is a block-diagonal matrix defined by

$$\mathcal{R}_{ij}^w = W_{ij}(0) \oplus \left(\bigoplus_{p=1}^f \begin{bmatrix} \Re\{W_{ij}(j\omega_p)\} & \Im\{W_{ij}(j\omega_p)\} \\ -\Im\{W_{ij}(j\omega_p)\} & \Re\{W_{ij}(j\omega_p)\} \end{bmatrix} \right), \quad (11)$$

and $W_{ij}(s) = \mathcal{L}\{w_{ij}(t)\}$.

Remark 6. Note that, following Lemma 2, each ω_p in (9) represents a desired interpolation point for the model reduction process, i.e. a frequency where the transfer function of system $\Sigma_{\mathcal{G}}$ matches the transfer function of the original system Σ .

Remark 7. The set \mathcal{F} , as defined in this study, inherently incorporates the zero element, i.e. we always consider matching at $s = 0$. This is particularly useful for a proper parameterisation of the radiation force subsystem, as it helps to enforce underlying physical properties (see Section 4).

EQUATIONS OF MOTION FOR A MULTI-DoF WEC

We now introduce the key concepts behind linear modelling of multi-DoF WECs, both in the time and frequency domains. The assumptions considered herein are consistent across a wide variety of WEC control/estimation studies such as (Faedo et al., 2018c, 2019, Li and Belmont, 2014, Peña-Sanchez et al., 2018).

Equations in the time domain

The motion for a WEC with N DoF can be expressed in the time-domain according to Newton's second law, obtaining the following linear hydrodynamic formulation:

$$M\ddot{\chi}(t) = \mathcal{F}_r(t) + \mathcal{F}_h(t) + \mathcal{F}_e(t), \quad (12)$$

where $M = \bigoplus_{i=1}^N m_i$ is the mass matrix of the buoy with $m_i \in \mathbb{R}^+$ the mass of the i -th DoF, and the elements of the vectors $\chi, \mathcal{F}_e, \mathcal{F}_h, \mathcal{F}_r \in \mathbb{R}^N$ contain the excursion $x_i(t)$, excitation force $f_{e_i}(t)$, hydrostatic restoring force $f_{h_i}(t)$ and radiation force $f_{r_i}(t)$ acting on the i -th DoF, with $i \in \mathbb{N}_N$, respectively.

The linearised hydrostatic force $\mathcal{F}_h(t)$ can be written as $-S_h\chi(t)$, where the matrix $S_h \in \mathbb{R}^{N \times N}$ is defined as $S_h = \sum_{i=1}^N \sum_{j=1}^N e_{ij}^N \otimes s_{h_{ij}}$ and contains the hydrostatic stiffness of each DoF (if $i = j$) and each interaction between the different modes of motion of the device due to the movement of each other DoF (if $i \neq j$). The radiation force $\mathcal{F}_r(t)$ is modelled from linear potential theory and, using Cummins' equation (Cummins, 1962), is

$$\mathcal{F}_r(t) = -\mu_\infty \ddot{\chi}(t) - \int_0^{+\infty} K(\tau) \dot{\chi}(t - \tau) d\tau, \quad (13)$$

where $\mu_\infty = \lim_{\omega \rightarrow +\infty} A(\omega)$ represents the added-mass matrix at infinite frequency (Falnes, 2002) and $K(t) = \sum_{i=1}^N \sum_{j=1}^N e_{ij}^N \otimes k_{ij}(t) \in \mathbb{R}^{N \times N}$, $k_{ij}(t) \in L^2(\mathbb{R})$ contains the (causal) radiation impulse response of each DoF (if $i = j$) and each interaction due to radiated waves created by the motion of other DoF (if $i \neq j$).

Finally, we can express the linearised equation of motion of the multi-DoF WEC as

$$(M + \mu_\infty) \ddot{\chi}(t) + K(t) * \dot{\chi}(t) + S_h \chi(t) = \mathcal{F}_e(t). \quad (14)$$

Equations in the frequency domain

Applying the Fourier transform to (14), and considering the velocity of each DoF a measurable output i.e. $\dot{\chi}(t)$, the following representation

$$\hat{\dot{\chi}}(j\omega) = \hat{\mathcal{F}}_e(j\omega) H(j\omega), \quad (15)$$

where $H : \mathbb{C}^0 \rightarrow \mathbb{C}^{N \times N}$ denotes the force-to-velocity frequency response mapping of the WEC, holds. The mapping $H(j\omega)$ can be readily computed (Falnes, 2002) as

$$H(j\omega) = \left(B(\omega) + j\omega(A(\omega) + M) - \frac{S_h}{j\omega} \right)^{-1}, \quad (16)$$

where $B(\omega)$ and $A(\omega)$ represent the radiation damping, and the radiation added mass matrix of the device, respectively. These

parameters are calculated using hydrodynamic codes at a finite set of uniformly spaced frequency samples $\Omega = \{\omega_i\}_{i=1}^M$ with $\Omega \subset [\omega_l, \omega_u]$, where ω_l and ω_u represents the lower and upper bound of the range, respectively. We note that the ideal frequency range depends explicitly on the application, as discussed in (Faedo et al., 2018b).

Mapping between time and frequency

Following the study performed in (Ogilvie, 1964), we recall that there exists a straightforward relation between the parameters of the models (14) and (15), which can be readily obtained via a direct application of the Fourier transform as

$$B(\omega) = \int_0^{+\infty} K(t) \cos(\omega t) dt, \quad (17)$$

$$A(\omega) = \mu_\infty - \frac{1}{\omega} \int_0^{+\infty} K(t) \sin(\omega t) dt.$$

Then, the radiation force impulse response mapping $K : \mathbb{R}^+ \rightarrow \mathbb{R}^{N \times N}$ can be directly written (Falnes, 2002) as

$$K(t) = \frac{2}{\pi} \int_0^{+\infty} B(\omega) \cos(\omega t) d\omega. \quad (18)$$

Considering equation (18), the frequency-domain representation of the radiation force kernel $K(t)$ can be obtained in terms of its Fourier transform $K(j\omega)$, i.e.

$$K(j\omega) = B(\omega) + j\omega [A(\omega) - \mu_\infty]. \quad (19)$$

The radiation kernel frequency response $K(j\omega)$ has a set of particular properties, which have been used in the literature to enforce a structure on the parametric model used to identify the frequency domain data. Such properties are recalled from (Pérez and Fossen, 2008) in Table 1.

Property	Significance on K
I) $\lim_{\omega \rightarrow +\infty} K(j\omega) = 0$	Strictly proper
II) $\lim_{t \rightarrow +\infty} K(t) = 0$	BIBO stable
III) $\lim_{\omega \rightarrow 0} K(j\omega) = 0$	It has transmission zeros ³ at the origin
IV) $\Re\{K_{ii}(j\omega)\} > 0, \forall i \in \mathbb{N}_N$	Passivity ⁴

Table 1 Properties of the radiation kernel K .

MOMENT-BASED RADIATION SYSTEM

The radiation impulse response mapping defines a linear-time invariant system completely characterised by $K : \mathbb{R}^+ \rightarrow \mathbb{R}^{N \times N}$, where its input is the vector containing the device velocities for each DoF, i.e. $\dot{\chi}(t)$. To be precise, the radiation subsystem Σ^K is given by

$$\Sigma_K : \theta_K(t) = K(t) * \dot{\chi}(t), \quad (20)$$

where $\theta_K(t) \in \mathbb{R}^N$ is the output (radiation force) of system Σ_K .

With the definition of Σ_K , and following the theory presented in Section 2, we can obtain a parametric model $\tilde{\Sigma}_{K, \mathcal{F}}$ for the radiation force subsystem defined in (20) using the result of Lemma

³See Khalil (1996) for the definition of a transmission zero.

⁴See Khalil (1996) for a proof concerning the passivity condition on the diagonal elements of $K(j\omega)$.

2, which offers an explicit computation of the moment-domain equivalent of a system in terms of its impulse response mapping. To that end, and in the spirit of Assumption 1, we express the velocity of the multi-DoF WEC $\dot{\chi}(t)$ as an autonomous multiple-output signal generator in a similar fashion to \mathcal{G} in (4), i.e.

$$\mathcal{G}_{\dot{\chi}} : \{\dot{\Xi}_{\dot{\chi}}(t) = (\mathbb{I}_N \otimes S) \Xi_{\dot{\chi}}(t), \quad \dot{\chi}(t) = L_{\dot{\chi}} \Xi_{\dot{\chi}}(t), \quad (21)$$

with S as in (9), $\dot{\Xi}_{\dot{\chi}}(0) = [1 \ \epsilon_{\nu-1}^\top]^\top$ and $L_{\dot{\chi}}$ such that the pair $(L_{\dot{\chi}}, S)$ is observable. Then, recalling the result of Lemma 2, the moment-domain equivalent of the output of system Σ_K in (20) can be straightforwardly computed as

$$\underline{\mathcal{Y}}_K = \sum_{i=1}^N \sum_{j=1}^N \epsilon_{ij}^N L_{\dot{\chi}} (\mathbb{I}_N \otimes \mathcal{R}_{ij}^k), \quad (22)$$

where each $\mathcal{R}_{ij}^k \in \mathbb{R}^{\nu \times \nu}$ is a block-diagonal matrix defined by

$$\mathcal{R}_{ij}^k = 0 \oplus \left(\bigoplus_{p=1}^f \begin{bmatrix} \Re\{K_{ij}(j\omega_p)\} & \Im\{K_{ij}(j\omega_p)\} \\ -\Im\{K_{ij}(j\omega_p)\} & \Re\{K_{ij}(j\omega_p)\} \end{bmatrix} \right). \quad (23)$$

Note that each entry of \mathcal{R}_{ij}^k directly depends on the hydrodynamic coefficients computed with BEM solvers. To be precise, let $A_{ij}(\omega)$ and $B_{ij}(\omega)$ be the ij -th element of the added mass matrix $A(\omega)$ and the radiation damping matrix $B(\omega)$ of the device, respectively. Then,

$$\begin{aligned} \Re\{K_{ij}(j\omega_p)\} &= B_{ij}(\omega_p), \\ \Im\{K_{ij}(j\omega_p)\} &= \omega_p [A_{ij}(\omega_p) - \mu_{\infty, ij}], \end{aligned} \quad (24)$$

where $\mu_{\infty, ij}$ is the ij -th element of the matrix μ_∞ .

Remark 8. Note that each matrix \mathcal{R}_{ij}^k already incorporates the hydrodynamic property $K_{ij}(0) = 0$ (see Table 1, Property III).

Finally, following Definition 2 and Lemma 1, we note that the parametric (state-space) description

$$\tilde{\Sigma}_{K, \mathcal{F}} : \{\dot{\Theta}_K(t) = F_K \Theta_K(t) + G_K \chi(t), \quad \tilde{\theta}_K(t) = Q_K \Theta_K(t), \quad (25)$$

is a system that interpolates the target frequency response $K(j\omega)$ at the set \mathcal{F} , i.e. it has the *exact* same frequency response of the radiation subsystem Σ_K at the frequencies defined in the set \mathcal{F} , if $Q_K P_K = \underline{\mathcal{Y}}_K$, where $P_K \in \mathbb{R}^{\nu \times \nu}$ is the unique solution of the Sylvester equation

$$F_K P_K + G_K L_{\dot{\chi}} = P_K (\mathbb{I}_N \otimes S), \quad (26)$$

and $\underline{\mathcal{Y}}_K$ is computed from equation (22). The explicit computation of the matrices F_K, G_K, Q_K in (25) (fulfilling condition (26)) is addressed in the following section.

MODELS ACHIEVING MOMENT-MATCHING

Herein, we briefly summarise some of the key concepts behind the algorithm proposed in (Peña-Sanchez et al., 2019) to compute a moment-based time-domain model for an array of WECs, and we adapt the procedure for our multi-DoF radiation force subsystem case. We note that (Peña-Sanchez et al., 2019) regards the moment-based concepts described in this study in synergy with well-known results of subspace-based identification methods, as detailed in (McKelvey et al., 1996).

To be precise, we approximate the dynamic and output matrix from the target radiation subsystem Σ_K in terms of the corresponding singular value decomposition of the Hankel matrix \mathcal{H}

(see (McKelvey et al., 1996)), constructed from $K(j\omega)$ as defined in (19) and computed at the finite set of uniformly spaced frequencies Ω (see Section 3). This α -dimensional approximated matrices ${}^d\hat{A}_\alpha \in \mathbb{R}^{\alpha \times \alpha}$, $\hat{C}_\alpha \in \mathbb{R}^{N \times \alpha}$ (where ${}^d\hat{A}_\alpha$ corresponds to a discrete-time model) can be computed⁵ as

$${}^d\hat{A}_\alpha = (J_1 \hat{U}_\alpha)^\dagger J_2 \hat{U}_\alpha, \quad \hat{C}_\alpha = J_3 \hat{U}_\alpha. \quad (27)$$

where the continuous-time equivalent matrix \hat{A}_α can be obtained directly from ${}^d\hat{A}_\alpha$ using, for instance, the bilinear transformation.

Remark 9. If ${}^d\hat{A}_\alpha$, computed as in (27), has unstable eigenvalues, one can always project such a set into the complex unit circle following the procedure described in (McKelvey et al., 1996).

Finally, the moment-based identification algorithm for the radiation force subsystem utilised herein can be summarised in the following steps:

- I ◦ Select a set of f interpolation points (frequencies ω_p) $\mathcal{F} = 0 \cup \{\omega_p\}_{p=1}^f$ to achieve moment-matching.
- II ◦ Compute the matrix $\mathbb{I}_N \otimes S$ following (9) and select any $L_{\dot{\chi}}$ such that the pair $(L_{\dot{\chi}}, \mathbb{I}_N \otimes S)$ is observable.
- III ◦ Calculate the moment-domain equivalent of the output of system (20) $\underline{\mathcal{Y}}_K$ using equation (22).
- IV ◦ Compute the matrices $\hat{A}_{N\nu}$ and $\hat{C}_{N\nu}$ from (27)⁶.
- V ◦ Consider the parametric model for the radiation subsystem described in (25) and set $F_K = \hat{A}_{N\nu}$ and $Q_K = \hat{C}_{N\nu}$.
- VI ◦ Consider the frequency response of (25), i.e.

$$\tilde{K}(j\omega, G_K) = Q_K (j\omega_i - F_K)^{-1} G_K$$

Using the frequency set $\Omega = \{\omega_i\}_{i=1}^M$, compute the input matrix G_K^{opt} with the following optimisation-based procedure:

$$G_K^{\text{opt}} = \arg \min_{G_K} \sum_{i=1}^M \left\| \tilde{K}(j\omega_i, G_K) - K(j\omega_i) \right\|_F^2$$

subject to:

$$F_K P_K + G_K L_{\dot{\chi}} = P_K (\mathbb{I}_N \otimes S),$$

$$Q_K P_K = \underline{\mathcal{Y}}_K.$$

- VII ◦ Compute a $N\nu$ -dimensional radiation force subsystem time-domain model $\tilde{\Sigma}_{K\mathcal{F}}$ achieving moment-matching at S as

$$\tilde{\Sigma}_{K\mathcal{F}} : \begin{cases} \dot{\Theta}_K(t) = F_K \Theta_K(t) + G_K^{\text{opt}} \dot{\chi}(t), \\ \tilde{\theta}_K(t) = Q_K \Theta_K(t). \end{cases}$$

Remark 10. The method is based on the idea of building the model $\tilde{\Sigma}_{K\mathcal{F}}$ by matching the $f + 1$ (user defined) frequencies of the set \mathcal{F} , exploiting the system structure of (25), and solving for an equality-constrained optimisation problem, which computes the input matrix G_φ^{opt} that minimises the difference between the target frequency response and that of (25), while ensuring the moment-matching conditions in the model.

APPLICATION TO A CORPOWER-LIKE DEVICE

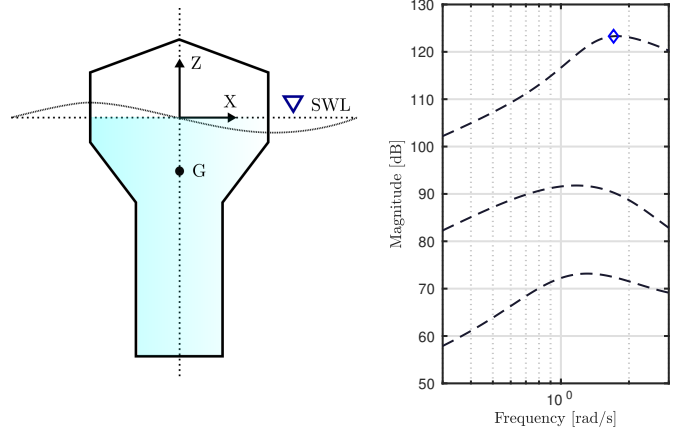
To illustrate the strategy proposed in this study, we consider the CorPower⁷-like device utilised in (Giorgi and Ringwood, 2019),

⁵We refer the reader to (McKelvey et al., 1996) for the explicit expression of the matrices J_1, J_2, J_3 and \hat{U}_α .

⁶We note that standard MATLAB routines can be used to obtain $\hat{A}_{N\nu}$ and $\hat{C}_{N\nu}$ from the frequency-domain data $K(j\omega)$.

⁷See (CorPower, 2019) for more detail on the CorPower device.

and depicted herein in Figure 1a. We refer the reader to (Giorgi and Ringwood, 2019) for a precise description of the dimensions of this device.



(a) Schematic of the device (b) Singular values plot for $K(j\omega)$

Fig. 1 CorPower-like device considered in this study.

Following the analysis carried out in (Giorgi and Ringwood, 2019), we consider *surge* (mode 1), *heave* (mode 2) and *pitch* (mode 3) as the more relevant DoF for this particular application case. The corresponding hydrodynamic parameters $A(\omega)$ and $B(\omega)$ can be appreciated in Figure 2. Note that the elements $\{1, 2\}, \{2, 1\}, \{2, 3\}, \{3, 2\}$ of the matrices $A(\omega)$ and $B(\omega)$ are not shown in Figure 2, given that there is no interaction due to radiation forces between these particular modes of motions, i.e. they are exactly zero for all $\omega \in \mathbb{R}^+$. The maximum frequency selected in the BEM code, to compute the hydrodynamic parameters of the CorPower-like device of Figure 2, is set to 10 [rad/s]. Nevertheless, we note that ocean waves peak periods typically lie between 3 [s] and 16 [s], which implies that the frequency range of the wave excitation force \mathcal{F}_e is approximately [0.4, 2.1] [rad/s] (Faedo et al., 2018b). Hence, it is straightforward to conclude that, under the modelling assumptions considered in Section 3, the velocity of the multi-DoF device (input to Σ_K) has significant frequency components in the same range.

From now on, we denote the frequency-domain model of the radiation subsystem corresponding to our CorPower-like device $K(j\omega)$ as the *target* response. In addition, we use the notation $K_{ij}(j\omega)$ for the ij -element of the matrix $K(j\omega)$. More precisely, $K_{ij} : \mathbb{C}^0 \rightarrow \mathbb{C}$ is the frequency response mapping between the output i (radiation force exerted on the i -th mode) and the input j (velocity of the j -th mode).

Approximation of the radiation subsystem

We now specifically proceed with the computation of a moment-based approximation $\tilde{\Sigma}_{K\mathcal{F}}$ for the radiation subsystem Σ_K , based on the knowledge of the target frequency response $K(j\omega)$, and using the procedure described in Section 5.

Recall that the first step of the algorithm is to select the set of frequencies \mathcal{F} to interpolate. In the SISO case (1-DoF device) of (Faedo et al., 2018b), a sensible choice can be made by analysing the gain of $K(j\omega)$, and selecting dynamically important points, such as the resonant frequency of the particular DoF under study,

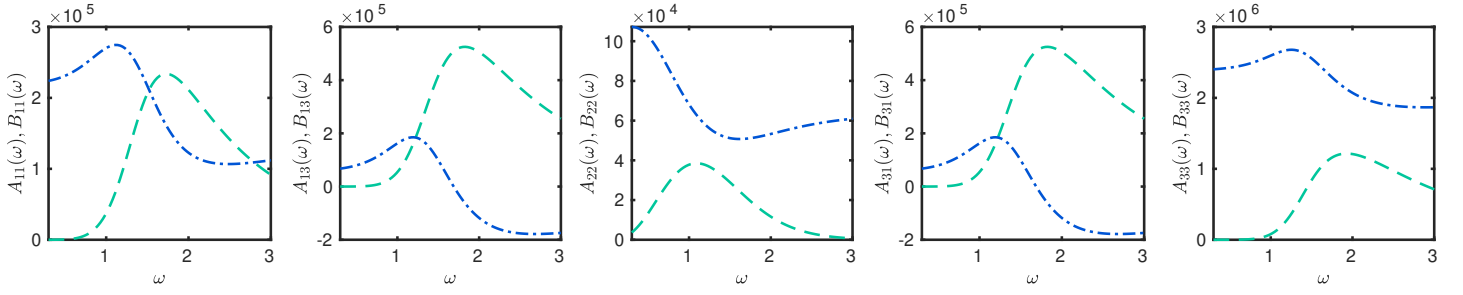


Fig. 2 Hydrodynamic parameters $A(\omega)$ (dot-dashed blue) and $B(\omega)$ (dashed green) for the CorPower-like device considered herein.

i.e. where the maximum amplification occurs. For this MIMO case, it is well-known that the system gain depends on the corresponding input direction (see, for example, (Zhou and Doyle, 1998)), so that this set of dynamically important points cannot be obtained by inspecting each element $K_{ij}(j\omega)$ independently. Instead, we use the *singular values* of $K(j\omega)$ (Zhou and Doyle, 1998), which are plotted in Figure 1b.

Following well-known theory for MIMO systems, it is straightforward to notice, from Figure 1b, that $\omega \approx 1.7$ [rad/s] represents an interpolation point of dynamical importance (marked with a blue-diamond in Figure 1b), being the frequency where the maximum amplification occurs, i.e. the frequency characterising the \mathcal{H}_∞ -norm of the system (Zhou and Doyle, 1998).

Based on this, we propose two different frequency interpolation sets \mathcal{F} , as follows:

$$\mathcal{F}_1 = \{0, 1.7\}, \quad \mathcal{F}_2 = \{0, 0.8, 1.7\},$$

where \mathcal{F}_2 includes the set \mathcal{F}_1 and incorporates an additional low frequency component $\omega = 0.8$ [rad/s]. Note that both sets include the zero element (see Remark 7). Following the discussion provided at the beginning of this section, the frequency range selected to approximate $K(j\omega)$ is given by $\Omega = [0.3, 3]$ [rad/s], with a frequency discretisation step of 0.01 [rad/s]. Given that heave (mode 2) is the main DoF of this WEC, Figure 3 presents the Bode diagram for the target response $K_{22}(j\omega)$ (dashed-black), and the moment-based approximated response $\tilde{K}_{22}(j\omega)$ (solid-gray), for both parametric models $\tilde{\Sigma}_{K\mathcal{F}_1}$ (left) and $\tilde{\Sigma}_{K\mathcal{F}_2}$ (right). The interpolation points for each model are denoted by an empty red circle. As expected, the approximated systems have the *exact* same frequency response as the target model for each corresponding set \mathcal{F} . Though using the set \mathcal{F}_1 as interpolation set provides quite accurate results, the decrease in the approximation error from system $\tilde{\Sigma}_{K\mathcal{F}_1}$ to $\tilde{\Sigma}_{K\mathcal{F}_2}$ can be clearly appreciated.

As a conclusive graphical illustration of the frequency-domain performance for the models computed via our strategy, Figure 4 presents the singular value plot for the target response $K(j\omega)$, and the approximated mapping $\tilde{K}(j\omega)$, both for $\tilde{\Sigma}_{K\mathcal{F}_1}$ (left) and $\tilde{\Sigma}_{K\mathcal{F}_2}$ (right). It can be readily appreciated that both models can accurately approximate the target singular values in every principal direction, i.e. the target MIMO gain, with an increase in accuracy when using the interpolation set \mathcal{F}_2 instead of \mathcal{F}_1 .

To illustrate the case of time-domain simulations, Figure 5 (left axis) presents the time-domain response of the parametric model $\tilde{\Sigma}_{K\mathcal{F}_2}$, along with the corresponding target steady-state response for the radiation subsystem of the CorPower-like device computed from $K(j\omega)$. It can be appreciated how, after the transient response of system $\tilde{\Sigma}_{K\mathcal{F}_2}$ extinguishes, each of the steady-state

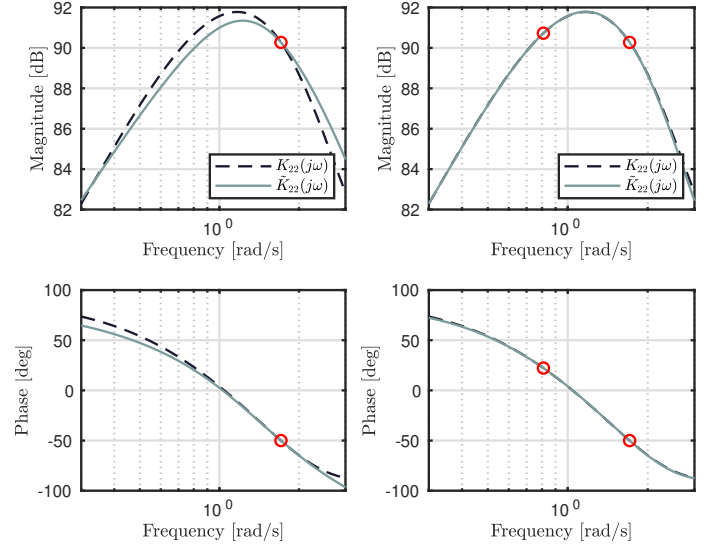


Fig. 3 Bode diagram for $K_{22}(j\omega)$ (dashed-black), and $\tilde{K}_{22}(j\omega)$ (solid-gray), for both parametric models $\tilde{\Sigma}_{K\mathcal{F}_1}$ (left) and $\tilde{\Sigma}_{K\mathcal{F}_2}$ (right). The interpolation points are denoted by an empty red circle

outputs of the approximating model behaves almost identically to its corresponding target output. Note that Figure 5 (right axis) also offers the exact input (velocity) used to simulate such a response.

Aiming to further assess the strategy, Table 2 offers a numerical appraisal of each of the moment-matching based parametric models in terms of the following parameters:

Dim: Dimension (order) of the parametric model

NRMSE_F: Normalized Root Mean Square Error (NRMSE) computed against the target WEC frequency response $\forall \omega \in \Omega$.

NRMSE_T: NRMSE computed (in steady-state) against the target steady-state radiation system response using inputs generated with frequency content inside the set Ω . In order to get meaningful results for the time-domain scenario of Table 2, and since the inputs are generated from sets of random amplitudes, it is found that the mean of 10 simulations is necessary to obtain a 95% confidence interval with a half-width of 0.25% of the mean, computed as in (Peña-Sanchez et al., 2018).

The first row of Table 2 includes the “multi-SISO”, which corresponds to a parametric model of the MIMO system Σ_K obtained

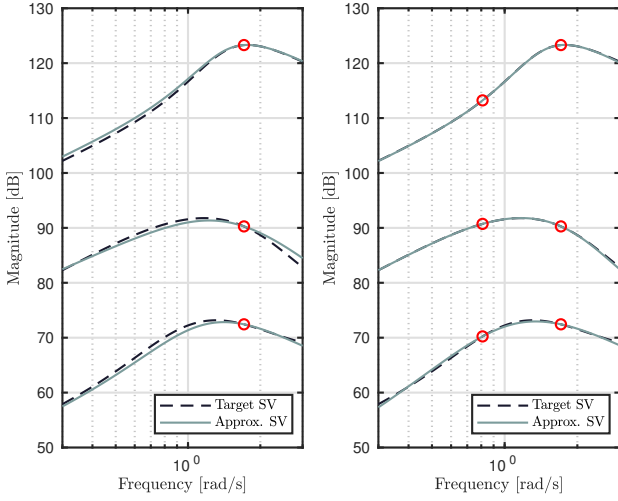


Fig. 4 Singular value (SV) plot for $K(j\omega)$ (dashed-black) and $\tilde{K}(j\omega)$ (solid-gray). The interpolation points are denoted by an empty red circle.

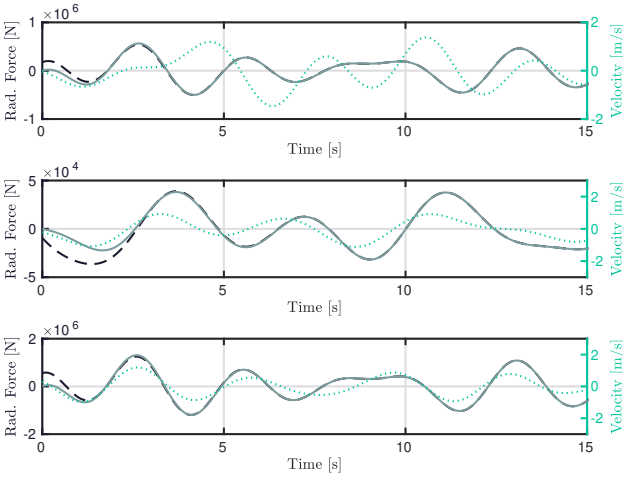


Fig. 5 Time-domain response (left axis) of $\tilde{\Sigma}_{K\mathcal{F}_2}$ (solid gray) along with the corresponding target steady-state response computed from $K(j\omega)$ (dashed black). The right axis offers the exact input (velocity) used to elicit such a response (dotted green).

by approximating each individual element of the matrix $K(j\omega)$ with a SISO system. The strategy used to compute this previously discussed model is the SISO moment-matching method described in (Faedo et al., 2018b) (with \mathcal{F}_2 as interpolation points), resulting in a model of dimension 25.

It is noteworthy to highlight that, as can be appreciated in Table 2, the approach proposed herein provides highly accurate results even with a single interpolation point (in addition to the zero frequency), with only $\approx 4\%$ of error in both the frequency- and time-domain, and with an intrinsic decrease in computational complexity, given the low dimension (order) of the resulting model. We also note that the “multi-SISO” approach provides similar results to those of $\tilde{\Sigma}_{K\mathcal{F}_2}$ with higher computational requirements (i.e.

Model	Dim	NRMSE _F	NRMSE _T
“multi-SISO”	28	1.036%	0.985%
$\tilde{\Sigma}_{\mathcal{F}_1}$	9	3.580%	4.045%
$\tilde{\Sigma}_{\mathcal{F}_2}$	15	1.092%	0.664%

Table 2 Numerical comparison table.

higher system order). That said, we emphasize that the radiation subsystem should be treated as a MIMO system when it comes to its parametric approximation.

To conclude the assessment of our strategy, we analyse the moment-based computed models $\tilde{\Sigma}_{K\mathcal{F}}$ with respect to the physical properties of the radiation subsystem listed in Table 1.

- *Property I* (Σ_K is strictly proper): this property is always fulfilled by the family of parametric models defined in (25), see, for example, (Khalil, 1996).
- *Property II* (Σ_K is BIBO stable): the strategy proposed in Section 5 preserves the dynamic matrix approximated using the Hankel matrix associated with $K(j\omega)$. This matrix can always be constructed so that is Hurwitz (see Remark 10) and, hence, system $\tilde{\Sigma}_{K\mathcal{F}}$ is BIBO stable. By way of example, Figure 6 shows the pole-zero map for system $\tilde{\Sigma}_{K\mathcal{F}_1}$ computed in this same section for the CorPower-like device. It can be appreciated that all the poles are contained in the open left-half of the complex plane, i.e. $\tilde{\Sigma}_{K\mathcal{F}_1}$ is BIBO stable.

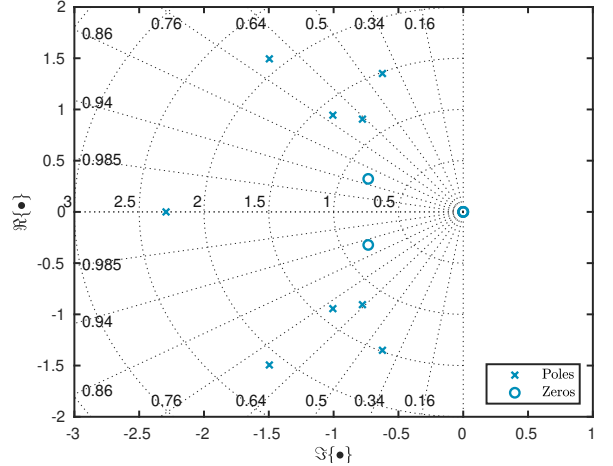


Fig. 6 Pole-zero map for the approximating model $\tilde{\Sigma}_{K\mathcal{F}_1}$.

- *Property III* (Σ_K has transmission zeros at $s = 0$): this property is specifically enforced by considering 0 as part of the set of interpolation points \mathcal{F} (see Remark 8). In practice, this can be (graphically) appreciated in the pole-zero map of Figure 6, where the zero at $s = 0$ manifests explicitly for the approximating model $\tilde{\Sigma}_{K\mathcal{F}_1}$.
- *Property IV* (Σ_K is passive): this particular physical property is not enforced by our strategy. However, we note that, if the target data $K(j\omega)$ effectively comes from a passive model⁸,

⁸This is clarified since errors can manifest in BEM codes, producing hydrodynamic coefficients that correspond to a non-passive system. For further discussion, see (Faedo et al., 2018b).

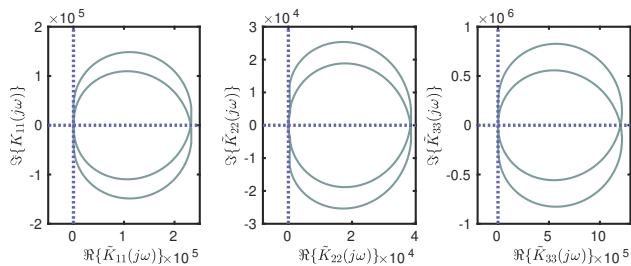


Fig. 7 Nyquist plot (diagonal elements) of $\tilde{K}(j\omega)$ for $\tilde{\Sigma}_{K\mathcal{F}_2}$.

the parametric models computed with our strategy, for the WEC radiation force subsystem, are virtually inherently passive⁹. Figure 7 depicts the Nyquist plot for the diagonal elements of $\tilde{K}(j\omega)$ for $\tilde{\Sigma}_{K\mathcal{F}_2}$, where it can be appreciated that $\Re\{\tilde{K}_{ii}(j\omega)\} > 0$ for all $i \in \mathbb{N}_3$ and, hence, $\Sigma_{K\mathcal{F}_2}$ is passive.

CONCLUSIONS

This paper presents a MIMO moment-based identification framework for the radiation force subsystem of multi-DoF WECs. The proposed strategy computes a parametric model of the target radiation force mapping using raw frequency-domain data produced by well-known BEM-based hydrodynamic codes. Such a moment-based model *exactly* matches the target steady-state response for a user-defined set of frequencies, allowing for the preservation of the relevant dynamic characteristics of the device. Moreover, we show that this parametric approximation retains important properties of radiation forces, such as input-output stability and passivity, agreeing with the underlying physics that characterise such a system. The performance of the strategy is demonstrated and analysed from both a time- and a frequency-domain perspective, using a CorPower-like multi-DoF device as application case.

ACKNOWLEDGMENT

The authors thank Prof. Alessandro Astolfi and Dr. Giordano Scarciotti from Imperial College London, for useful discussions on moments. This material is based upon works supported by Science Foundation Ireland under Grant no. 13/IA/1886.

REFERENCES

Antoulas, A. C. (2005). *Approximation of large-scale dynamical systems*. SIAM.

Astolfi, A. (2010). Model reduction by moment matching for linear and nonlinear systems. *IEEE Transactions on Automatic Control*, 55(10), 2321–2336.

CorPower (2019). *The CorPower Wave Energy Converter*. URL: <http://www.corpowerocean.com/>, Accessed January 10.

Cummins, W. E. (1962). The impulse response function and ship motions. *Schiffstechnik*, 47, 101–109.

Faedo, N., Olaya, S., and Ringwood, J. V. (2017). Optimal control, MPC and MPC-like algorithms for wave energy systems: An overview. *IFAC Journal of Systems and Control*, 1, 37–56.

Faedo, N., Peña Sanchez, Y., and Ringwood, J. V. (2018a). Passivity preserving moment-based finite-order hydrodynamic

⁹We note that, if required by the application, a similar strategy to that of (Faedo et al., 2018a) can be considered to specifically ensure passivity within this multi-DoF moment-based framework.

model identification for wave energy applications. In *Advances in Renewable Energies Offshore, RENEW 2018*, 351–359.

Faedo, N., Peña-Sanchez, Y., and Ringwood, J. V. (2018b). Finite-order hydrodynamic model determination for wave energy applications using moment-matching. *Ocean Engineering*, 163, 251 – 263.

Faedo, N., Scarciotti, G., Astolfi, A., and Ringwood, J. V. (2018c). Energy-maximising control of wave energy converters using a moment-domain representation. *Control Engineering Practice*, 81, 85 – 96.

Faedo, N., Scarciotti, G., Astolfi, A., and Ringwood, J. V. (2019). Moment-based constrained optimal control of an array of wave energy converters. In *2019 American Control Conference (ACC), Philadelphia*.

Falnes, J. (2002). *Ocean waves and oscillating systems: linear interactions including wave-energy extraction*. Cambridge University Press.

Giorgi, G. and Ringwood, J. V. (2019). A compact 6-dof nonlinear wave energy device model for power assessment and control investigations. *IEEE Transactions on Sustainable Energy*, 10(1), 119–126.

Hals, J., Falnes, J., and Moan, T. (2011). Constrained optimal control of a heaving buoy wave-energy converter. *Journal of Offshore Mechanics and Arctic Engineering*, 133(1), 011401.

Khalil, H. K. (1996). *Nonlinear Systems*. Prentice-Hall, New Jersey.

Li, G. and Belmont, M. R. (2014). Model predictive control of sea wave energy converters—part II: The case of an array of devices. *Renewable Energy*, 68, 540–549.

McKelvey, T., Akçay, H., and Ljung, L. (1996). Subspace-based multivariable system identification from frequency response data. *IEEE Transactions on Automatic Control*, 41(7), 960–979.

Ogilvie, T. F. (1964). Recent progress toward the understanding and prediction of ship motions. In *5th Symposium on naval hydrodynamics*, 2–5. Bergen, Norway.

Padoan, A., Scarciotti, G., and Astolfi, A. (2017). A geometric characterization of the persistence of excitation condition for the solutions of autonomous systems. *IEEE Transactions on Automatic Control*, 62(11), 5666–5677.

Peña-Sanchez, Y., Faedo, N., and Ringwood, J. V. (2019). Moment-based parametric identification of arrays of wave energy converters. In *2019 American Control Conference (ACC), Philadelphia*.

Peña-Sanchez, Y., Garcia-Abril, M., Paparella, F., and Ringwood, J. V. (2018). Estimation and forecasting of excitation force for arrays of wave energy devices. *IEEE Transactions on Sustainable Energy*, 9(4), 1672–1680.

Penalba, M., Kelly, T., and Ringwood, J. V. (2017). Using NEMOH for modelling wave energy converters: A comparative study with WAMIT. In *Proceedings of the 12th European Wave and Tidal Energy Conference, Cork*, 631.

Pérez, T. and Fossen, T. I. (2008). Time-vs. frequency-domain identification of parametric radiation force models for marine structures at zero speed. *Modeling, Identification and Control*, 29(1), 1–19.

Scarciotti, G. and Astolfi, A. (2017). Nonlinear model reduction by moment matching. *Foundations and Trends in Systems and Control*, 4(3–4), 224–409.

Zhou, K. and Doyle, J. C. (1998). *Essentials of robust control*, volume 104. Prentice hall Upper Saddle River, NJ.